

PCCP

Accepted Manuscript



This is an *Accepted Manuscript*, which has been through the Royal Society of Chemistry peer review process and has been accepted for publication.

Accepted Manuscripts are published online shortly after acceptance, before technical editing, formatting and proof reading. Using this free service, authors can make their results available to the community, in citable form, before we publish the edited article. We will replace this *Accepted Manuscript* with the edited and formatted *Advance Article* as soon as it is available.

You can find more information about *Accepted Manuscripts* in the [Information for Authors](#).

Please note that technical editing may introduce minor changes to the text and/or graphics, which may alter content. The journal's standard [Terms & Conditions](#) and the [Ethical guidelines](#) still apply. In no event shall the Royal Society of Chemistry be held responsible for any errors or omissions in this *Accepted Manuscript* or any consequences arising from the use of any information it contains.

Inquiry of the Electron Density Transfers in Chemical Reactions. Complete Reaction path for the Denitrogenation Process of 2,3 diazabicyclo[2.2.1]hept-2-ene Derivatives

Vicent S. Safont,¹ Patricio González-Navarrete,^{1,2} Mónica Oliva¹ and Juan Andrés¹

¹Departamento de Química Física y Analítica, Universitat Jaume I, Avda. Sos Baynat s/n, 12071, Castelló de la Plana, Spain.

² Author present address: Institut für Chemie, Technische Universität Berlin Straße des 17 Juni 135, 10623 Berlin, Germany
E-mail: andres@qfa.uji.es

Abstract:

A detailed study on all stages associated with the reaction mechanisms for the denitrogenation of 2,3 diazabicyclo[2.2.1]hept-2-ene derivatives (DBX, with X substituents at the methano-bridge carbon atom, X= H, OH) is presented. In particular, we have characterized the processes leading to cycloalkene derivatives through *migration-type* mechanisms as well as the processes leading to cyclopentil-1,3-diradical species along *concerted* or *stepwise* pathways. The reaction mechanisms have been further analysed within the bonding evolution theory framework at B3LYP and M05-2X/6-311+G(2d,p) level of the theory. Analysis of the results allows us to obtain the intimate electronic mechanism for the studied processes, providing a new topological picture of processes underlying a correlation between the experimental measurements obtained by few-optical-cycle visible pulse radiation and the quantum topological analysis of the electron localization function (ELF) in terms of breaking/forming processes along this chemical rearrangement. The evolution of the population of the disynaptic basin $V(N1,N2)$ can be related with the experimental observation associated with the N=N stretching mode evolution, relative to the N_2 release, along the reaction process. This result allows us to determine why the N_2 release is easier for the DBH case via a *concerted* mechanism compared to the *stepwise* mechanism found in DBOH system. This holds the key to unprecedented insight into the mapping of the electrons making/breaking the bonds while the bonds change.

Keywords: Electron Localization Function, Bonding Evolution Theory, Reaction Mechanism, Denitrogenation Processes.

1. Introduction

One of the key challenges in chemistry has been to characterize and then to understand the breaking and formation of chemical bonds along the course of a given chemical reaction. For such purpose, a reaction mechanism describes in detail what is exactly happening at each stage (elementary reaction) of an overall chemical process (transformation) and, even more specifically, which bonds break (in the reactant) and form (in the product) along the reaction coordinate. Hence, the knowledge of the atom–atom mapping certainly constitutes the foundation for its establishing. In addition, chemical kinetics measurements have had a crucial role in determining unknown chemical processes, providing rate laws and rate constants that can then be used to derive a plausible reaction mechanism. Nevertheless, in some cases the elementary steps of a given reaction mechanism cannot be identified unambiguously since they are not experimentally accessible requiring the complement of a theoretical description for such complex chemical rearrangements.

Certainly, visualizing the progress of chemical reactions on their natural time scale can be considered the holy grail of chemical physics giving rise to the whole description of the reaction mechanism. Experimentally, the reaction path is difficult to map because it proceeds so quickly and therefore suitable spectroscopies are very demanding. In particular, some efforts have now been done by means of ultrafast electron diffraction or X-ray diffraction,¹ while advances in the area of attosecond physics² and real-time vibrational spectroscopy³⁻⁵ by a few femtosecond pulse laser have been recently achieved. By means of this technique, the ultrashort visible pulse excites vibrational modes coherently in the electronic ground state through the stimulated Raman processes which precedes the reaction in the electronic ground state like the thermal excitation under heating. In particular, the mechanism of denitrogenation for 2,3-diazabicyclo[2.2.1]hept-2-ene (DBH) derivatives has been investigated using a visible 5-fs pulse laser.³ There has been a long debate concerning a reasonable mechanism that describes this reaction because the product formation could be achieved through a *concerted* or a *stepwise* mechanism. Thus, the process has been widely studied,⁶⁻²¹ establishing that the corresponding reaction mechanism for the thermal denitrogenation depends on the nature of substituents at the methano-bridge carbon atom of the DBH structure.^{3, 18, 21, 22} For electron donating substituents (X=H, -SiR₃) the denitrogenation process takes place via a *concerted* mechanisms, whereas σ electron withdrawing substituents (X = -F, -OCH₂CH₃) gives rise to stepwise ones via a diazenyl diradical intermediates.^{3, 18, 21} The substituent effects have been explained based on computational studies in which the lowest electronic configuration of the singlet state of the resulting diradicals¹⁸ has been invoked.

Motivated by these studies, our intention with the present work has been to study in greater detail the reaction mechanism for the thermal denitrogenation processes of DBH and DBOH under

the domain of quantum chemical topology (QCT),²³ a subarea of quantum mechanics, based on the analysis of the gradient of a scalar functions, following the seminal work of Bader.^{24, 25} This represents an alternative to understand and describe chemical reactivity based on well-defined physical entities accessible from experiments, in this case on the charge distribution. In the framework of QCT, bonding evolution theory (BET) proposed by Krokidis et al.,²⁶ which combines the electronic localization function (ELF)^{27, 28} and Thom's catastrophe theory (CT)^{26, 29} has been employed to unravel reaction mechanism and substituent effects.³⁰⁻⁴² To obtain a trustworthy picture, one first must perform computational studies, and then post-process the complicated information encoded in the accurate wavefunction in a way that facilitates chemical interpretation where concepts from QCT are used to provide insight into molecular electronic structure and the changes in electronic structure that accompany chemical processes.

It is worth noting that an important feature of BET is the ability to observe the flow of the electron density as the reaction proceeds; in other words, BET allows monitoring a chemical rearrangement along the reaction coordinate. One example of that corresponds to the thermal degenerate Cope rearrangement of semibullvalene,⁴³ where BET is capable to adequately predict the order, direction, and asynchronicity of electron fluxes, providing rather valuable information of reaction mechanisms at elementary level. Thus, within the broad scope of both experimental and theoretical investigations, the interest has been focused on extracting information about the evolution of structure and energy along the reaction which may be insufficient to establish its electronic mechanism in detail. Indeed, certain vibrational modes can be directly associated with the presence of covalent bonds while their evolutions in the course of the reaction coordinate may be correlated with the information provided from the BET analysis, and hence, an analysis could be desirable in such cases where reactions are too complex or too fast to be measured at *in situ* conditions due to slow and/or insensitive experimental techniques.

This work aims to contribute to the discussion on the nature of the reaction mechanism for the denitrogenation process in DBH and DBOH systems, assessing the usefulness of BET protocol by comparing with previous results obtained by means of selective laser pulses experiments. Therefore, our focus is here to reach deeper insight on how electron density rearranges and how this rearrangement can be associated with chemical events such as the breaking/forming of chemical bonds, along the reaction progress. Thus, questions such as: (i) how could the electronic reorganization proceed along the reaction path, (ii) how this reorganization can be related with experimental data obtained by real-time vibrational spectroscopy?, (iii) how substituent effects (electron donating/withdrawing) are related with the electronic density flows, (iv) where and how do bond formation/breaking processes take place?, and (v) how the electronic reorganizations can be related with stepwise C–N bond cleavage *versus* concerted cleavage of the two C–N bonds?,

may be answered and, admittedly, such a task is ambitious, but our hope is to provide a useful entry point to the growing literature by presenting a digestible account of key results to-date.

The paper is organized as follows: section 2 describes the computational procedure, and section 3 contains the results and discussions concerning the structure, energetics and ELF-topological properties of the different DBH and DBHO denitrogenation processes. Finally, we summarize our main conclusions in section 4.

2. Computational Procedure

Quantum chemical calculation have been performed using the Gaussian 09 suite.⁴⁴ We have selected the B3LYP⁴⁵⁻⁴⁷ exchange-correlation functional for the geometry optimizations of DBH, whereas for DBOH system the M05-2X functional⁴⁸ was used. The 6-311+G(2d,p) basis set were employed for all atoms, while vibrational frequencies were calculated to characterize the structures as minimum or transition states (TSs) as well as to obtain the zero-point-point energy corrections. The capability of B3LYP/6-311+G(2d,p) level to properly describe the decomposition process of DBH has been demonstrated because it predicts the same activation barrier (after the spin projection, see below) than the one calculated at (6,6)CASPT2/6-31G(d)//(6,6)CASSCF level as performed by Houk et al²⁰. On the other hand, B3LYP was not chosen for the DBOH system because it does not reproduce the second C-N bond cleavage as the rate-determining step of the stepwise mechanism, while the use of M05-2X functional agrees with these results reported by Abe et al. by using UCCSD/6-31G(d) level¹⁹.

Starting from the TS, the intrinsic reaction coordinate (IRC)^{49, 50} pathway is traced to their corresponding associated reactant and products. A mass-weighted step of 0.05 amu^{1/2} bohr has been employed until the minimum was reached. For each point along the IRC, the wave function has been obtained and the ELF analysis has been performed by means of the TopMod package⁵¹ considering a cubical grid of stepsize smaller than 0.05 bohr. The ELF basins are visualized using the program Chimera.⁵² Due to the presence of diradical species along the IRC path, the stability of the wave function was checked according to the procedure described by Bauernschmitt and Ahlrichs.⁵³ For *open-shell* TS and/or intermediate obtained at UDFT level, the *broken symmetry*^{54, 55} approach has been used as an approximation for multireference treatment. In addition a triplet calculation is performed to obtain E_t , while the projected low spin energy E_{ls} is calculated with the formula:

$$E_{ls} = E_t + \frac{2[E_{bs} - E_t]}{[2 - \langle S^2 \rangle_{bs}]} \quad (1)$$

E_{bs} corresponds to the energy of the *broken-symmetry* calculation, while $\langle S^2 \rangle_{bs}$ value corresponds to the total spin operator for the *broken-symmetry* solution, ranging from 0 when the valence electrons are paired to 1 in the ideal case of noninteracting spin in equivalent orbitals.

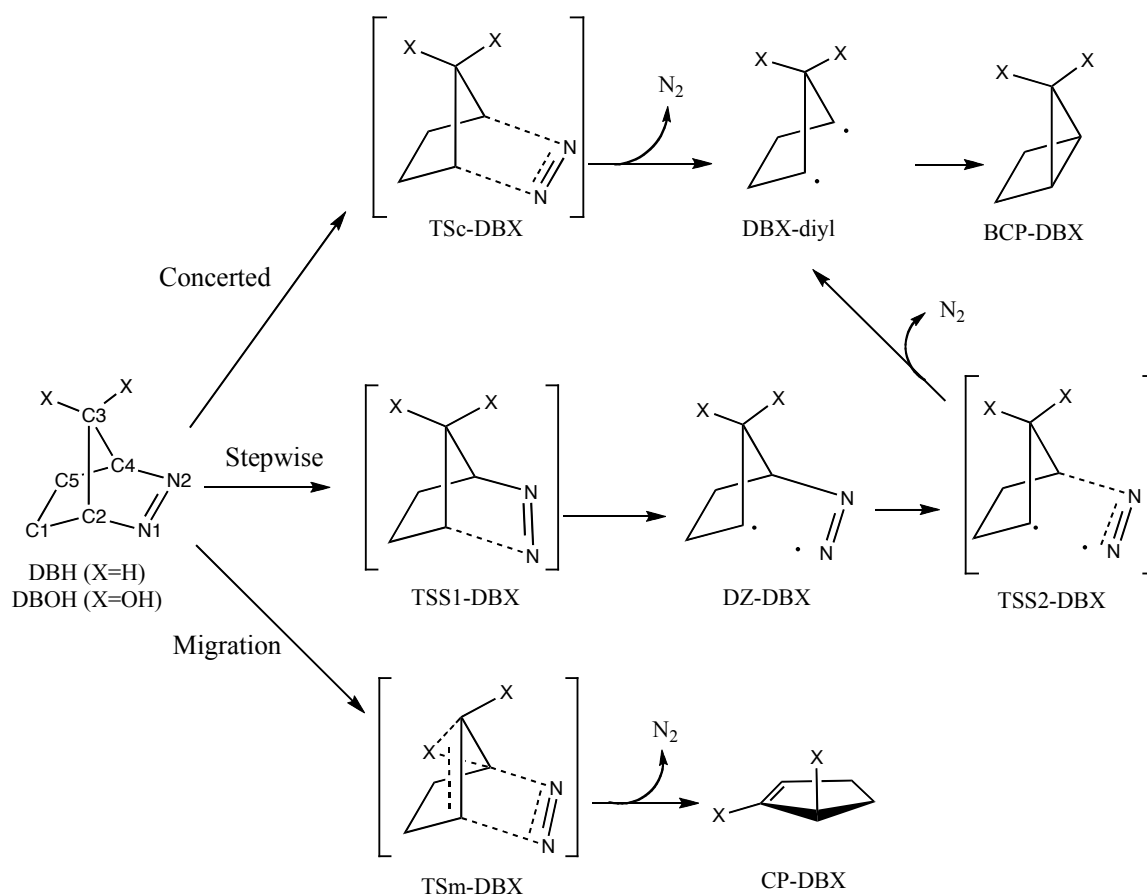
Previous theoretical studies have demonstrated that the ELF topological analysis is a valuable tool to gain fundamental insights from the breaking/forming processes along the reaction pathway.^{30-41, 43, 56, 57} The topological partition of the ELF gradient field²⁸ provides basin of attractors, which are classified as core and valence basins. Core basins $C(A)$ can be thought as atomic cores, while valence basins $V(A)$ can be interpreted as bond and lone pairs, where A is the atomic symbol of the element. $V(A)$, $V(A,B)$ or $V(A,B,C)$ are characterized by their coordination number with core basins (synaptic order) as monosynaptic, disynaptic or trisynaptic basins, respectively.⁵⁸ Thus, this description recovers the Lewis bonding model suggesting a graphical representation of the molecular system. A quantitative analysis is further achieved by integrating the electron density and the pair functions over the volume of the basin yielding basin populations (for details of the mathematical model of the ELF, see supporting information section).

Along a reaction pathway (which links the chemical structures and therefore the topologies of the ELF gradient fields of the reactants with those of the product) the system experiences a series of structural stability domains (SSDs) within which all the critical points are hyperbolic separated by catastrophic points at which at least one critical point is non-hyperbolic. The bifurcation catastrophes occurring at these turning points are identified according to Thom's classification²⁹ which gives access to their unfolding, a compact polynomial expression which contains all the information about how ELF may change as the control parameters change. In this way, a chemical reaction is viewed as a sequence of elementary chemical processes characterized by a catastrophe. These chemical processes are classified according to the variation of the number of basins μ and/or of the synaptic order σ of at least one basin. Details of the Thom's classification in chemical reactions have been described in detail elsewhere.⁵⁹

3. Results and Discussion

As stated before, the deazetization of DBH has been described as a *concerted* reaction mechanism giving rise to the cyclopentane 1,3-diyl species (DBH-diyl) via an *open-shell* singlet transition state (TSc-DBH), see Scheme 1. The *open-shell* singlet TSc-DBH is localized with an energy barrier of 37.1 kcal/mol and a $\langle S^2 \rangle$ value of 0.47. After the spin correction the energy barrier is predicted to be 32.3 kcal/mol, and in good agreement with previous energy barrier values reported, as aforementioned.^{3, 18, 20} This reaction pathway has been predicted to be endothermic when the system reaches the DBH-diyl diradical. At the same time, DBH-diyl has been proposed to be the intermediate species for the formation of the closed-shell bicycle [2.1.0]pentane (BCP-DBH).

The further steps from DBH-diyl to BCP-DBH fall outside the scope of the present work, and therefore we have not looked for the corresponding TS (or TSs). However, for the sake of completeness, the calculated values of energy for BCP-DBH are summarized in Table 1 and its geometries depicted in Figure 1. As expected, BCP-DBH lays more than 30 kcal/mol under DBH-diyl species, and therefore the whole process from DBH to BCP-DBH is predicted to be exothermic.



Scheme 1

Table 1. Relative (to DBH and DBOH in their closed-shell singlet state) energies (kcal/mol) of the stationary points found of the denitrogenation processes.

	DBH ^b		DBOH ^c
Species	<i>concerted</i> reaction pathway	Species	<i>stepwise</i> reaction pathway
DBH	0.0	DBOH	0.0
TSc-DBH ^a	37.1	TSS1-DBOH ^a	39.7
DBH-diyl ^a + N ₂	18.3	DZ-DBOH ^a	39.3
BCP-DBH + N ₂	-12.2	TSS2-DBOH ^a	41.7
	<i>migration</i> reaction pathway	DBOH-diyl ^a + N ₂	22.5
TSm-DBH	42.9	BCP-DBOH	-8.3
CP-DBH + N ₂	-43.5		<i>migration</i> reaction pathway
		TSm-DBOH	71.8
		CP-DBOH + N ₂	-37.6

^aOpen shell singlet species. ^bCalculated at B3LYP/6-311+G(2d,p) level. ^cCalculated at M05-2X/6-311+G(2d,p) level. Total energies of reactant species: DBH, -304,880853 hartrees/particle; DBOH, -455,332228 hartrees/particle.

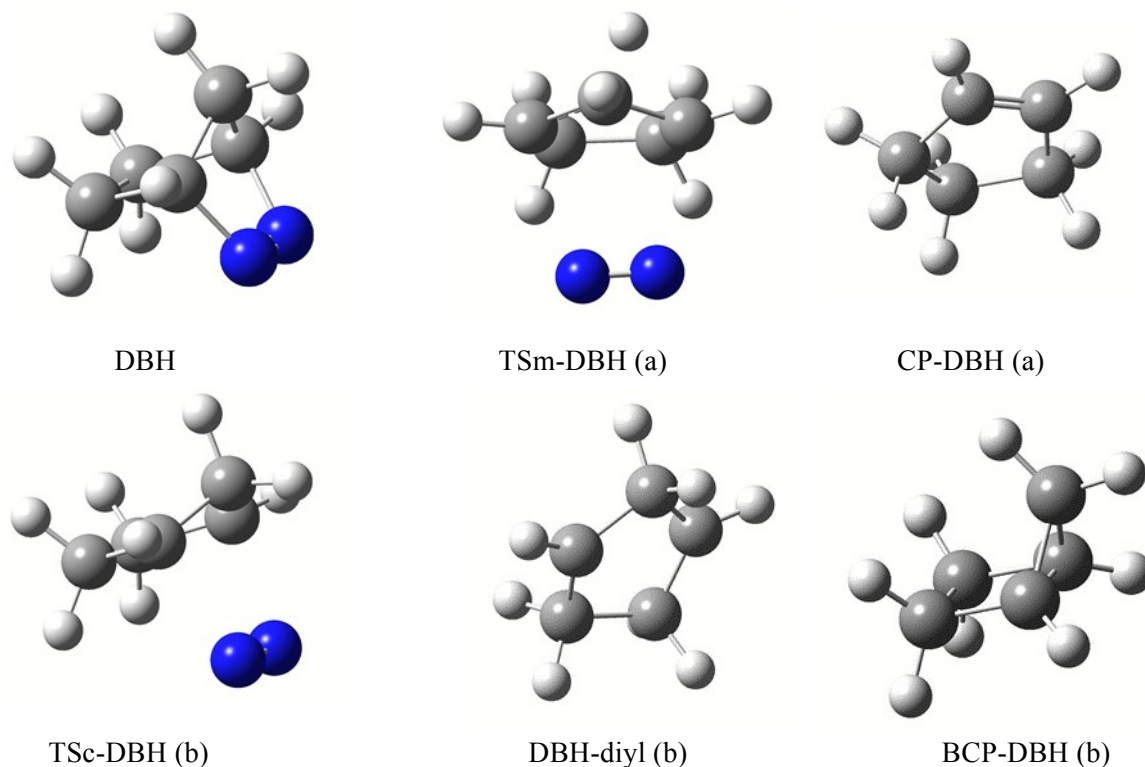


Figure 1. Stationary points of the denitrogenation of DBH via (a) *migration* reaction pathway, (b) *concerted* reaction pathway. Color code; blue: nitrogen; grey: carbon; white: hydrogen

In what refers to DBOH, B3LYP/6-31G(d) and CASSCF/6-31G(d) calculations^{3, 18, 20} predict the thermal denitrogenation of DBOH as a *stepwise* reaction mechanism where the first C2-N1 bond cleavage results in a Morse-like potential, giving rise to a low-lying diazenyl diradical intermediate (DZ-DBOH), see Scheme 1. In contrast, at UCCSD/6-31G(d) level, this TS associated with the first C2-N1 bond cleavage could be successfully optimized¹⁹ (TSS1-DBOH), and even, it was calculated to be lower than that TS associated with the C4-N2 cleavage, indicating that the rate-determining step of the process corresponds to the second C-N bond breaking.^{18, 19} Thus, the reaction mechanism proceeds by means of two TSs associated with the first and second C-N bond cleavages (TSS1-DBOH and TSS2-DBOH, respectively). Interestingly, an increase of the size of the basis set at M05-2X/6-311+G(2d,p) level allows the localization of the TS associated with the C2-N1 bond cleavage process, being thus consistent with UCCSD/6-31G(d) calculations. The respective energies of the localized species are summarized in Table 1, while its geometries are depicted in Figure 2. The *open-shell* singlet TSS1-DBOH and TSS2-DBOH are localized with

energy barrier of 39.7 and 41.7 kcal/mol; nevertheless after the spin correction the energy barriers are predicted to be 34.1 and 40.3 kcal/mol, in good agreement with previous energy barrier values reported.¹⁹ For comparison purposes, we also provide in supporting information (Tables 1S and 2S) the energetic values obtained by using the 6-31G(d) basis set for the reaction mechanisms studied for both systems, with both functionals.

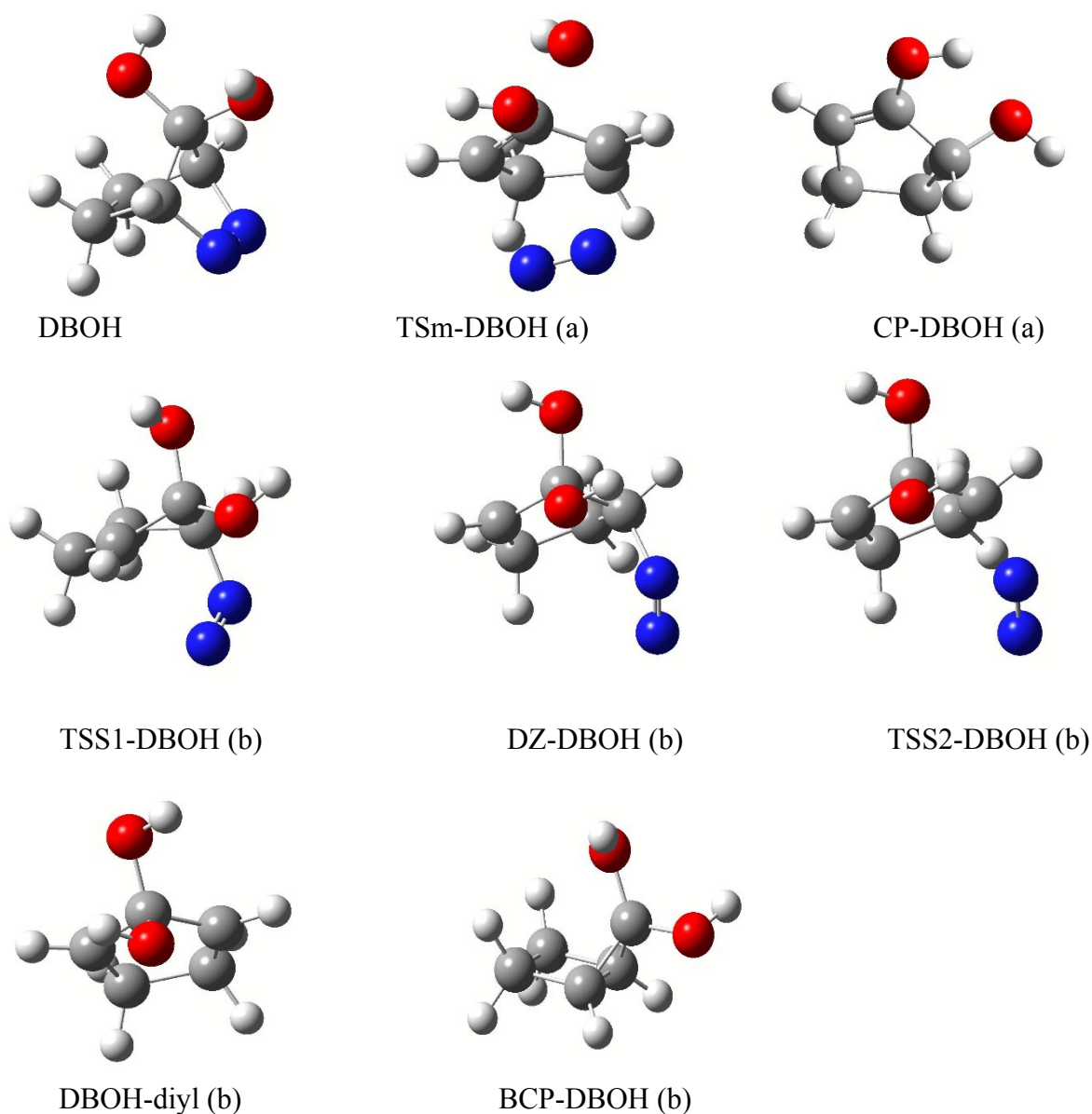


Figure 2. Stationary points of the denitrogenation of DBOH via (a) *migration* and (b) *stepwise* pathways. Color code; blue: nitrogen; red: oxygen; gray: carbon; white: hydrogen

On the other hand, it has also been reported the formation of cycloalquene products as result of an X migration process coupled with the N₂ departure (for instance, for X=OEt).¹⁹ Therefore, the *migration* reaction mechanisms have also been studied for DBH and DBOH. The migration reaction corresponds to a highly exothermic process and it takes entirely place via a *closed-shell* singlet state

via TSm-DBX giving rise to cyclopentene derivatives (CP-DBX). These results can be associated with the strain on the original bicycle system that relaxes with the N_2 departure and the formation of the stable cyclopentene. Likewise, a relatively high activation barrier has been predicted (for details see Table 1), accounting for the TS complexity: in a single step three single bonds are broken and three bonds are formed: one of them of single nature and the other two multiple. Therefore, both a fine tuning of the atom motions and a relatively high amount of energy are needed to reach the TSm-DBX. Thus, the activation barriers for DBH and DBOH have been predicted to be 43.0 kcal/mol and 72.0 kcal/mol, respectively. This complexity explains the difficulty in locating this kind of TS's either for the DBOH as well as for the X=OEt systems reported in the literature;¹⁹ we have for the first time characterized these elusive stationary points thus giving a full theoretical description for the migration pathways.

ELF Topological Description

a) Denitrogenation of DBH via *migration* reaction pathway

The IRC energy profile associated with the *migration* pathway is depicted in Figure 3 including six SSDs which are sketched in it from the perspective of the BET analysis: full lines and fat points represent disynaptic and monosynaptic basins, respectively, while hashed wedged bonds represent hydrogenated basins. The population of some basins along the IRC is shown in Figure 4. Snapshots of the ELF localization domains for some selected points along the IRC, representative of the different SSDs, are reported in supporting information (Figure 1S). In Figure 5 a selection of them are offered.

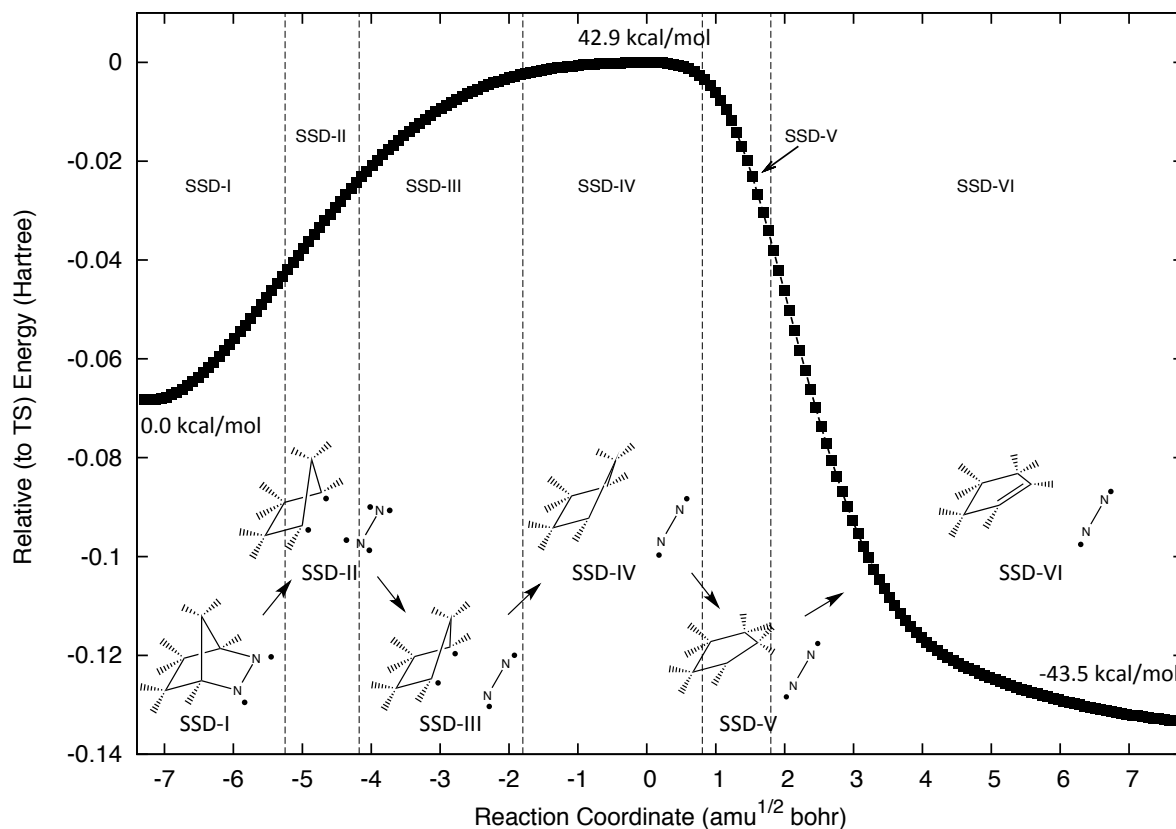


Figure 3. Energy profile of the denitrogenation of DBH (left side) to give CP-DBH species and N_2 (right side), with marked SSDs, whose topology is sketched, obtained from the BET analysis.

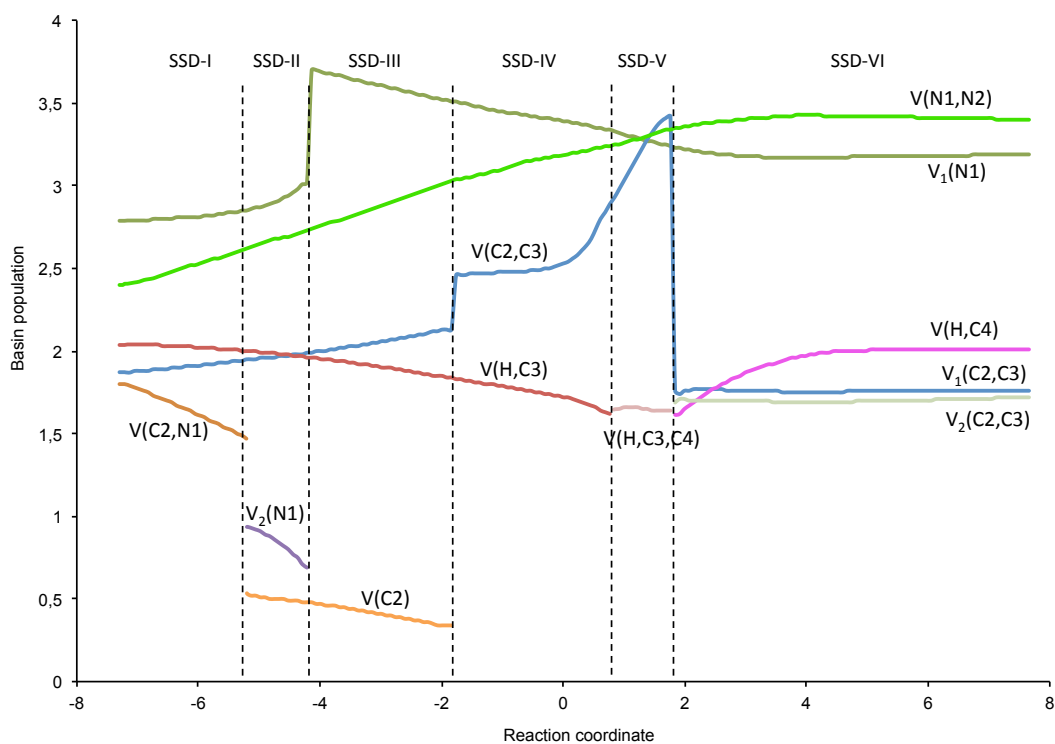


Figure 4. Population of some basins along the IRC path of the denitrogenation of DBH via migration reaction pathway as a function of the reaction coordinate ($\text{amu}^{1/2} \text{ bohr}$)

At the DBH species (left side of the energy profile in Figure 3), 25 basins have been localized: 7 core basins, 8 hydrogenated basins, 8 disynaptic basins accounting for the C-C, C-N and N-N bonds, and 2 monosynaptic basins ($V_1(N1)$ and $V_1(N2)$) accounting for the nitrogen lone pairs. The first ELF topological change (connecting SSD-I and SSD-II) comprises a simultaneous split of the disynaptic basins $V(C2,N1)$ and $V(C4,N2)$ by means of two simultaneous cusp-type catastrophes. As consequence, the SSD-II begins with the creation of 4 new monosynaptic basins ($V_2(N1)$, $V_2(N2)$, $V(C2)$, and $V(C4)$) whose total population equates the total one of the former disynaptic basins, surrounding their respective core basins (for comparison purposes see Figures 5a and 5b). In Figure 4 it can be sensed that the population of the disynaptic basin $V(C2,N1)$ decrease in the course of the SSD-I. The population of the $V(C4,N2)$ is always the same than the population of the $V(C2,N1)$ basin, so that it is not included. Along the SSD-II the populations of that four monosynaptic basins diminish, being more acute those of the monosynaptic basins $V_2(N1)$ (and $V_2(N2)$, not shown because it is always the same) with a concomitant increase in the population of the monosynaptic basin $V_1(N1)$ (and $V_1(N2)$, not shown for the same reason). Later, the second ELF topological change connecting SSD-II and SSD-III shows the annihilation of the monosynaptic basins $V_2(N1)$ and $V_2(N2)$ accounting for a double fold-type catastrophe, while the monosynaptic basins $V_1(N1)$ and $V_1(N2)$ acquire their respective populations which is reflected in a sudden increase of their populations when the system reaches the SSD-III. The next ELF-topological event connecting SSD-III and SSD-IV corresponds to the simultaneous annihilation of the monosynaptic basins $V(C2)$ and $V(C4)$ accounting for a double fold-type catastrophe, while a sudden increase of the population of the disynaptic basin $V(C2,C3)$ is sensed in Figure 4. Then, in the course of the SSD-IV the populations of the monosynaptic basins $V_1(N1)$ and $V_1(N2)$ decrease while the population of disynaptic basin $V(C2,C3)$ greatly increases: this disynaptic basin is anticipating its looming transformation. The population of the $V(H,C3)$ basin continuously diminishes from the very beginning of the process, and when the system reaches the SSD-V, it becomes trisynaptic $V(C3,H,C4)$ indicating thus the hydride migration process from C3 towards C4 (see Figure 5c). Finally, the last ELF-topological change discloses the transformation of the trisynaptic basin $V(C3,H,C4)$ into disynaptic basin $V(H,C4)$, while the split of the disynaptic basin $V(C2,C3)$ into two disynaptic basins $V_{1,2}(C2,C3)$ (cusp-type catastrophe) is also observed. These changes can clearly be seen in Figure 4.

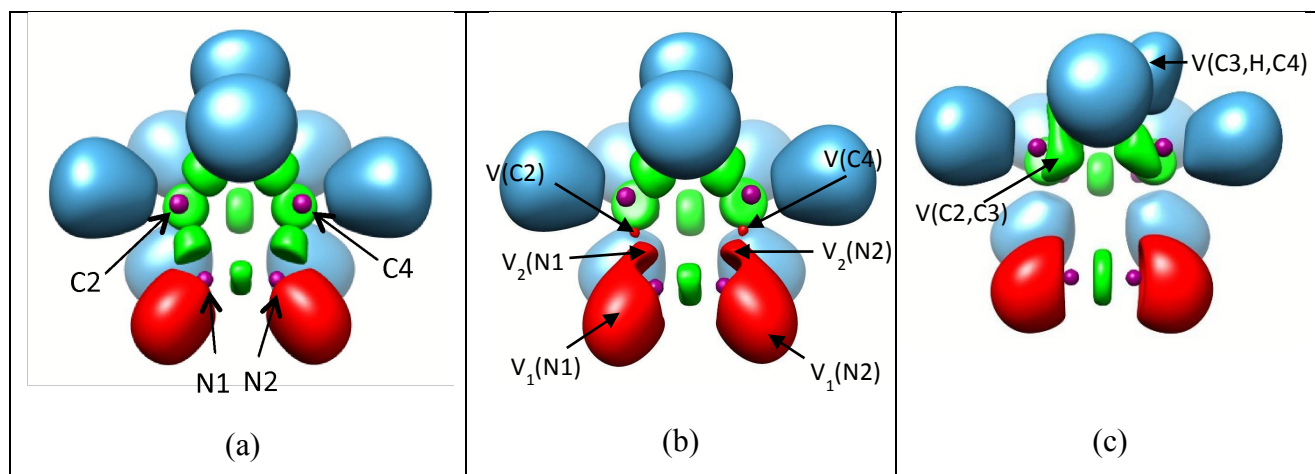


Figure 5. Snapshots of the ELF localization domains ($\eta = 0.8$ isosurface except where indicated) for selected points along the IRC of the denitrogenation of DBH via *migration* reaction pathway: (a) DBH belonging to SSD-I, (b) point at $s = -4.60 \text{ amu}^{1/2} \text{ bohr}$ ($\eta = 0.785$ isosurface) belonging to SSD-II, (c) point at $s = 1.69 \text{ amu}^{1/2} \text{ bohr}$ belonging to SSD-V. The color code is as follows: green, disynaptic basins; red, monosynaptic basins; blue, hydrogenated basins; purple, core basins.

Therefore, the description that emerges from the topological analysis of the DBH migration pathway reveals that the first chemical event that takes place is the simultaneous C-N bonds breaking, and it is not until the reaction has advanced halfway that the hydride migration becomes apparent. The formation of the double bond between C2 and C3 atoms is the last chemical event along the whole process, whose driving force can undoubtedly be assigned to the N_2 release. On the other hand, the population of the disynaptic $V(\text{N}_1, \text{N}_2)$ basin increases from 2.40e (at the DBH) up to 2.61e at the entrance of the SSD-II. Its population continues increasing along SSD-II, SSD-III, SSD-IV (for instance, it has a value of 3.18e at TSm-DBH) and SSD-V, and it is not until halfway the SSD-VI that it acquires a stable value around 3.40 e, very close to the value found for the N_2 molecule (3.36e).

b) Denitrogenation of DBH via *concerted* reaction pathway

The energy profile along the IRC for this pathway is depicted in Figure 6 including 4 SSDs which are sketched from the perspective of ELF analysis. The evolution of the basin populations along the IRC is shown in Figure 7, and snapshots of the ELF localization domains for some selected points along the IRC pathway, representative of some SSDs are presented in Figure 8. In Figure 2S (supporting information) snapshots of selected points representing all the SSDs found are reported.

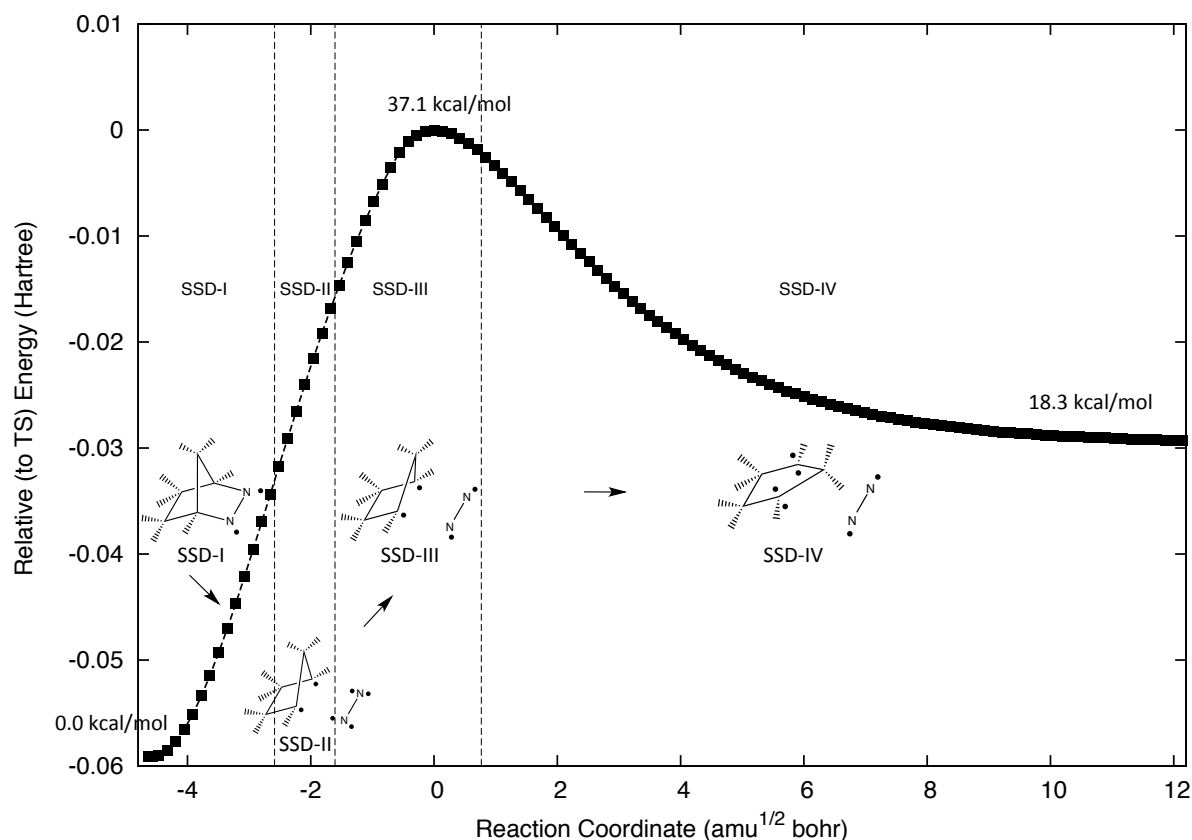


Figure 6. Energy profile of the denitrogenation of DBH (left side), to give DBH-diyl species and N_2 (right side), with marked SSDs whose topology is sketched, obtained from the BET analysis.

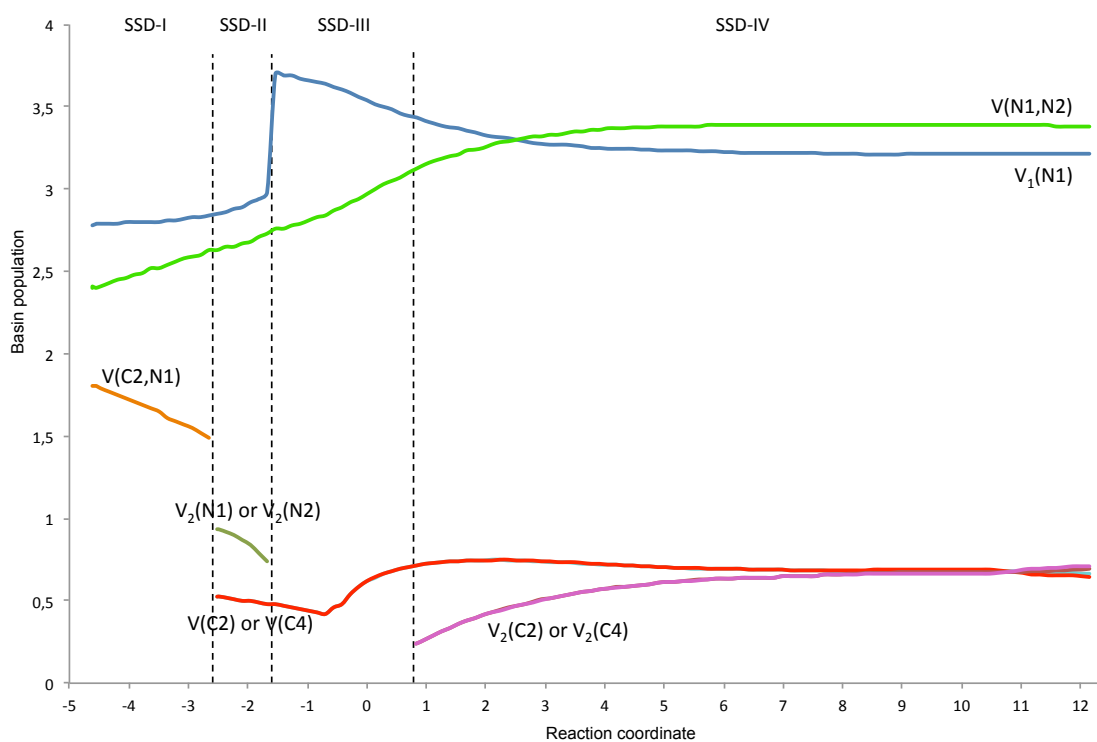
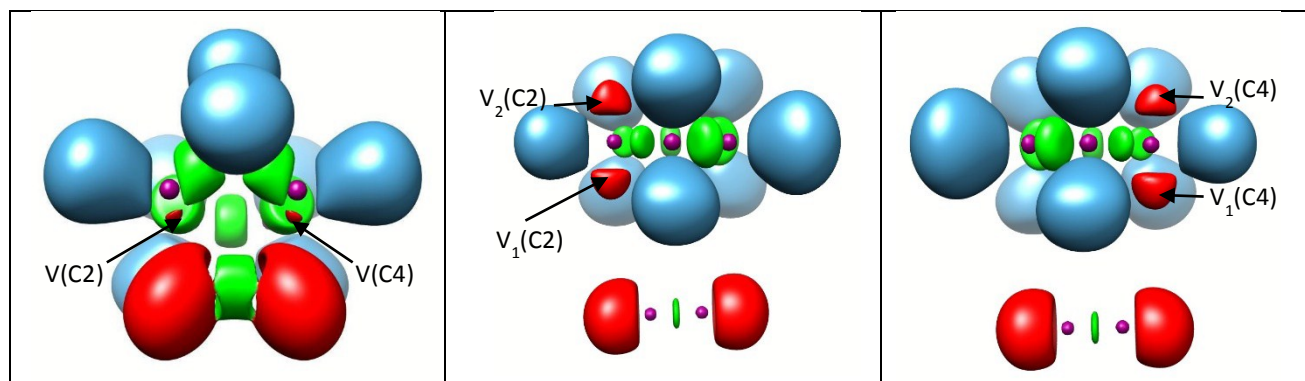


Figure 7. Population of some basins along the IRC path of the denitrogenation of DBH via *concerted* reaction pathway as a function of the reaction coordinate ($\text{amu}^{1/2} \text{ bohr}$)

Again, in this case the process begins with the simultaneous breaking of the two C-N bonds. The process undergoes the simultaneous split of the disynaptic basins $V(C2,N1)$ and $V(C4,N2)$ into four monosynaptic basins $V(C2)$, $V_2(N1)$, $V(C4)$ and $V_2(N2)$ by means of two cusp-type catastrophes. When the system reaches the SSD-III, the simultaneous annihilations of the monosynaptic basins $V_2(N1)$ and $V_2(N2)$ (fold-type catastrophe) are observed, see Figure 8a. The $V(N1,N2)$ basin population increases from 2.40e up to 2.63e at the end of SSD-I, then up to 2.97e at the TSc-DBH, and finally it reaches a stable value around 3.38e. Note that the topological evolution of the ELF field is practically identical to the migration reaction pathway until the system reaches the respective SSD-III; nevertheless is in the course of the SSD-III where the biradicaloid nature of the system is sensed. To avoid overlap between monosynaptic basins $V(C)$ and disynaptic basins $V(C-H)$ ^{37, 38, 60, 61} we have calculated the basin populations for α and β electrons separately. In the middle of the course of the SSD-III, the populations of the monosynaptic basins $V(C2)$ and $V(C4)$ increase accounting for a concentration of charge on C2 and C4 atoms. Finally, when the system reaches the SSD-IV, two fold-type of catastrophes are observed due to the creation of two monosynaptic basins $V_2(C2)$ and $V_2(C4)$. These two new monosynaptic basins appear as consequence of an excess of the charge density on C2 and C4 atoms indicating an electronic flux of the system towards these atoms (see Figure 7 for a detailed evolution of the basin populations).

It is evident that both denitrogenation mechanisms begin with the C-N bond cleavage processes. But certainly, the denitrogenation via *migration* pathway involves more chemical events (six SSDs), making this process energetically less favourable. Indeed, the charge density concentration between C2 and C3 atoms necessarily implies a hydride migration to reach the formation of CP-DBH and therefore this process needs a large energy to take place. In contrast, in the *concerted* mechanism the charge density flows directly towards C2 and C4 atoms upon the C-N bond cleavages, avoiding thus any additional internal chemical rearrangement. In consequence, the *concerted* reaction pathway allows a better electron density redistribution in the course of the process which is reflected in a more favourable energy demand compared to the *migration* rearrangement.



(a)	(b)	(c)
-----	-----	-----

Figure 8. Snapshots of some ELF localization domains for selected points along the IRC of the denitrogenation of DBH via *concerted* reaction pathway (see DBH belonging to SSD-I in Figure 5a): (a) TSc-DBH ($\eta=0.72$ isosurface) belonging to SSD-III, (b) point at $s=12.15$ $\text{amu}^{1/2}$ bohr ($\eta=0.86$ isosurface, alpha electrons) belonging to SSD-IV, (c) point at $s=12.15$ $\text{amu}^{1/2}$ bohr ($\eta=0.86$ isosurface, beta electrons) belonging to SSD-IV.

c) Denitrogenation of DBOH via *migration* reaction pathway

The energy profile along the IRC reaction pathway is depicted in Figure 9 including seven SSDs that are sketched according to the perspective of the BET analysis. Evolution of the basin populations along the IRC pathway is shown in Figure 10. Snapshots of some ELF-SSDs are presented in Figure 11, and the whole set of pictures can be found in Figure 3S (supporting information).

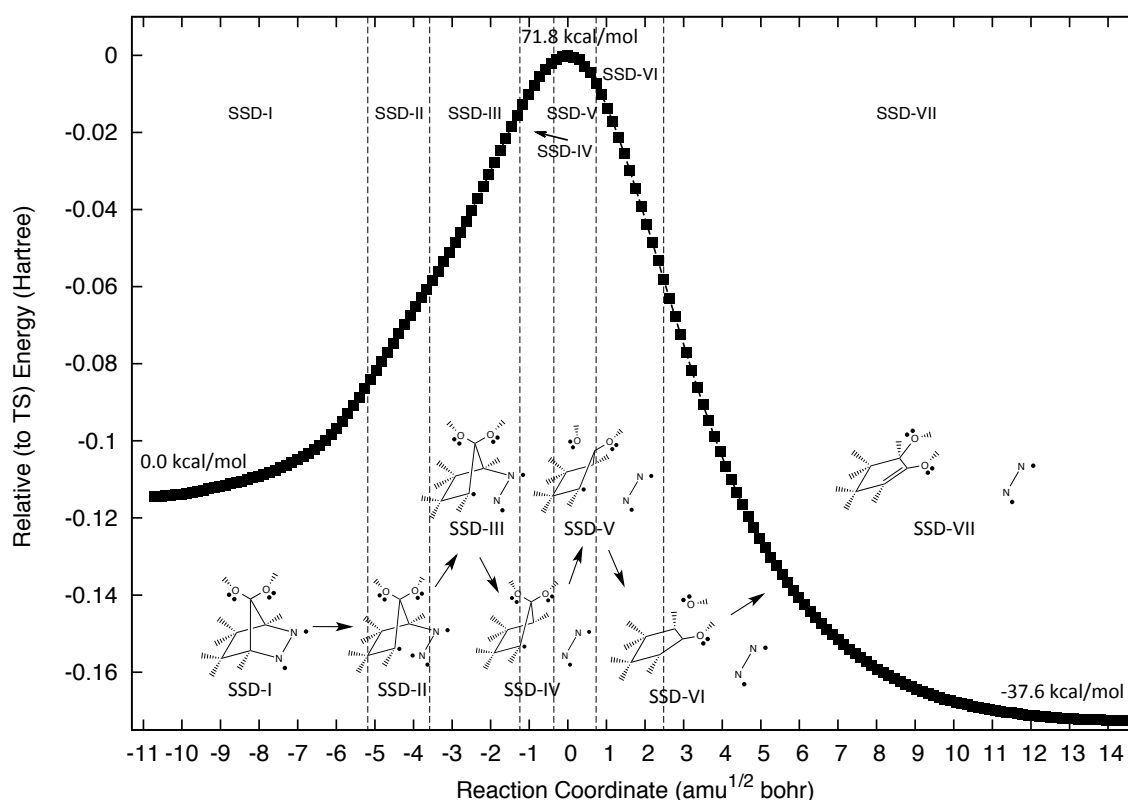


Figure 9. Energy profile of the denitrogenation of DBOH (left side), to give CP-DBOH species and N_2 (right side), with marked SSDs whose topology is sketched, obtained from the BET analysis.

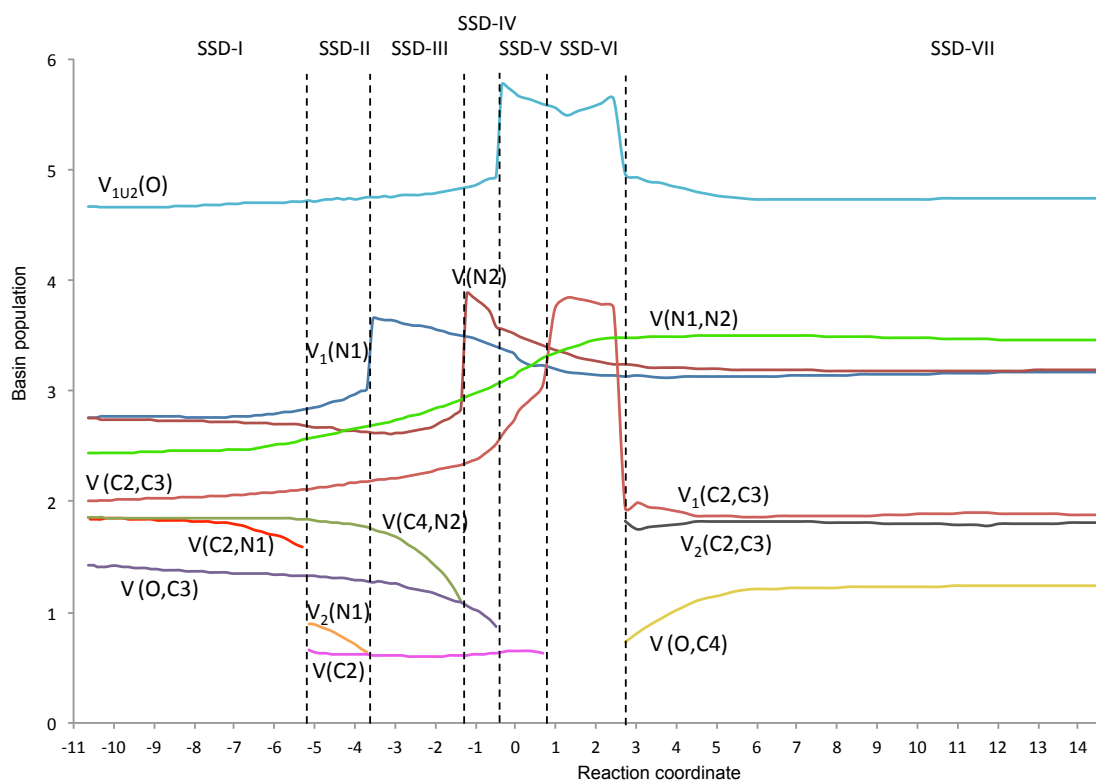


Figure 10. Population of some basins along the IRC path of the denitrogenation of DBOH via *migration* reaction pathway as a function of the reaction coordinate ($\text{amu}^{1/2} \text{ bohr}$).

As observed in Figure 9, the C-N bond cleavages do not occur simultaneously. Thus, the first ELF-topological change, connecting SSD-I and SSD-II, shows the split of the disynaptic basin $V(\text{C2},\text{N1})$ into two monosynaptic basins $V(\text{C2})$ and $V_2(\text{N1})$ by means of a cusp-type catastrophe. Then, in the course of the SSD-II the population of the monosynaptic basin $V(\text{C2})$ remains practically constant, whereas the population of the monosynaptic basin $V_2(\text{N1})$ diminishes. When the system reaches the SSD-III a fold-type catastrophe is observed accounting for the annihilation of the monosynaptic basin $V_2(\text{N1})$ (see Figure 11b); its population is now incorporated in the former monosynaptic basin $V_1(\text{N1})$ that experiences a sudden increase in its population, see Figure 10. In the course of the SSD-III the population of the disynaptic basin $V(\text{C2},\text{C3})$ slightly increases, while the pronounced diminution of the population of the disynaptic basin $V(\text{C4},\text{N2})$ finally ends up in the annihilation of this disynaptic basin when the system reaches the SSD-IV, by means of a fold-type catastrophe (see also Figure 11c); as consequence a sudden increase of the monosynaptic basin $V(\text{N2})$ is also sensed. Next, when the system reaches the SSD-V the ELF field undergoes a topological change disclosing the annihilation of the disynaptic basin $V(\text{O},\text{C3})$ (fold-type catastrophe) which accounts for the migration of the OH group from C3 towards C4; likewise an increase in the populations of the monosynaptic basins $V_{1,2}(\text{O})$, which belong to the mentioned OH group are observed. In Figure 10 the population of these two monosynaptic basins $V_{1,2}(\text{O})$ are

depicted as a whole ($V_{1U2}(O)$, see the pale blue line). Upon the annihilation of the disynaptic basin $V(O,C3)$, a diminution in the population of the basins $V(N2)$, $V_{1,2}(O)$ and $V_1(N1)$ is observed, accompanied with a pronounced increase in the population of the disynaptic basin $V(C2,C3)$. Subsequently, when the system reaches the SSD-VI, a fold-type catastrophe due to the annihilation of the monosynaptic basin $V(C2)$ is found, being its respective population transferred to the disynaptic basin $V(C2,C3)$. After that, a slight diminution in the population of the disynaptic basin $V(C2,C3)$ is sensed concomitantly with an increase in the sum of the population of the monosynaptic basins $V_{1,2}(O)$. When SSD-VII is reached, two simultaneous catastrophes occur: i) split of the disynaptic basin $V(C2,C3)$ into two disynaptic basins $V_{1,2}(C2,C3)$ accounts for the double character of the C2-C3 bond (cusp-type catastrophe) and ii) creation of the disynaptic basin $V(O,C4)$ (fold-type catastrophe), which reflects the migration process of the OH group. This last ELF topological change is accompanied by a diminution of the populations of the two monosynaptic basins $V_{1,2}(O)$. In addition, the population of the disynaptic basin $V(N1,N2)$ (see the light green line in Figure 10) reveals a slight increment in the early SSDs, but a more pronounced increase upon the annihilation of the disynaptic basin $V(C4,N2)$. Thus, when the system reaches the TS the population of the disynaptic basin $V(N1,N2)$ is predicted to be $3.18e$, reaching a stable value around $3.5e$ in the late SDDs. This value is roughly maintained along SSD-VII until the end of the IRC path, where a final population value of $3.46e$ is predicted.

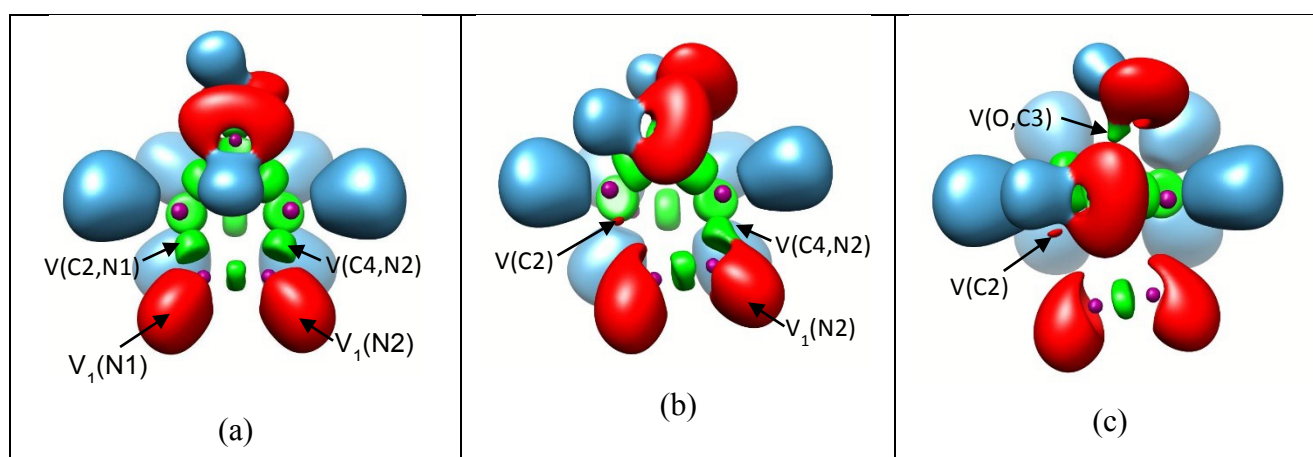


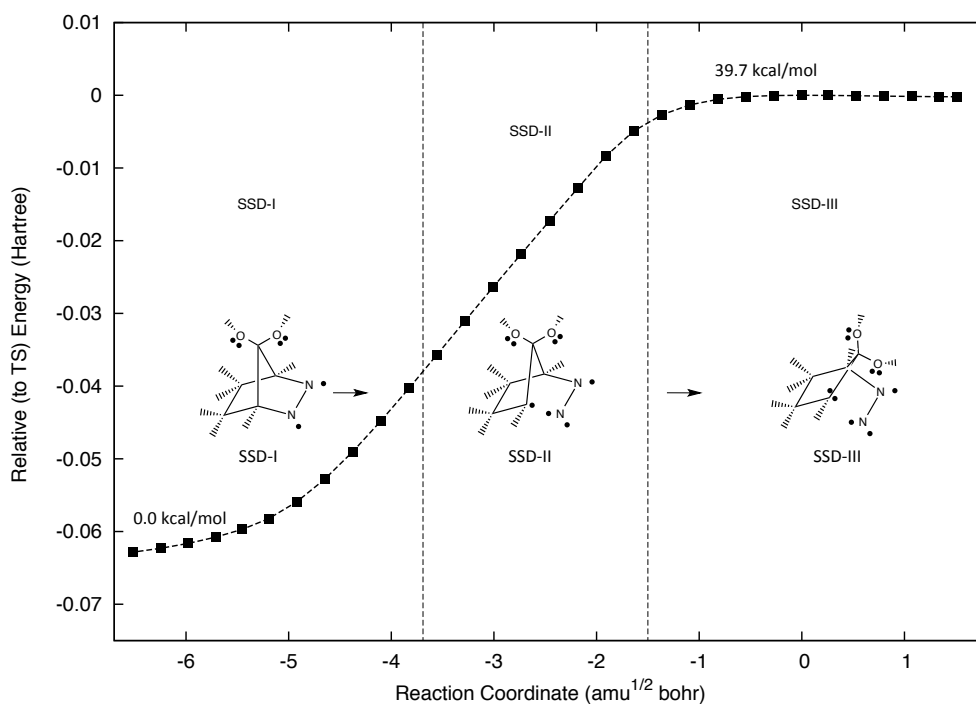
Figure 11. Snapshots of some ELF localization domains for selected points along the IRC of the denitrogenation of DBOH *via* the migration pathway: (a) DBOH belonging to the SSD-I domain ($\eta=0.8$ isosurface); (b) point at $s=-2.48 \text{ amu}^{1/2} \text{ bohr}$ belonging to SSD-III ($\eta=0.78$ isosurface); (c) point at $s=-0.88 \text{ amu}^{1/2} \text{ bohr}$ belonging to SSD-IV ($\eta=0.79$ isosurface).

A comparison can be done between DBH and DBOH migration processes. Certainly in the DBH case, the C-N bond cleavages take place simultaneously at the beginning of the process, giving rise directly to the hydride migration, and then to end up in the formation of CP-DBH.

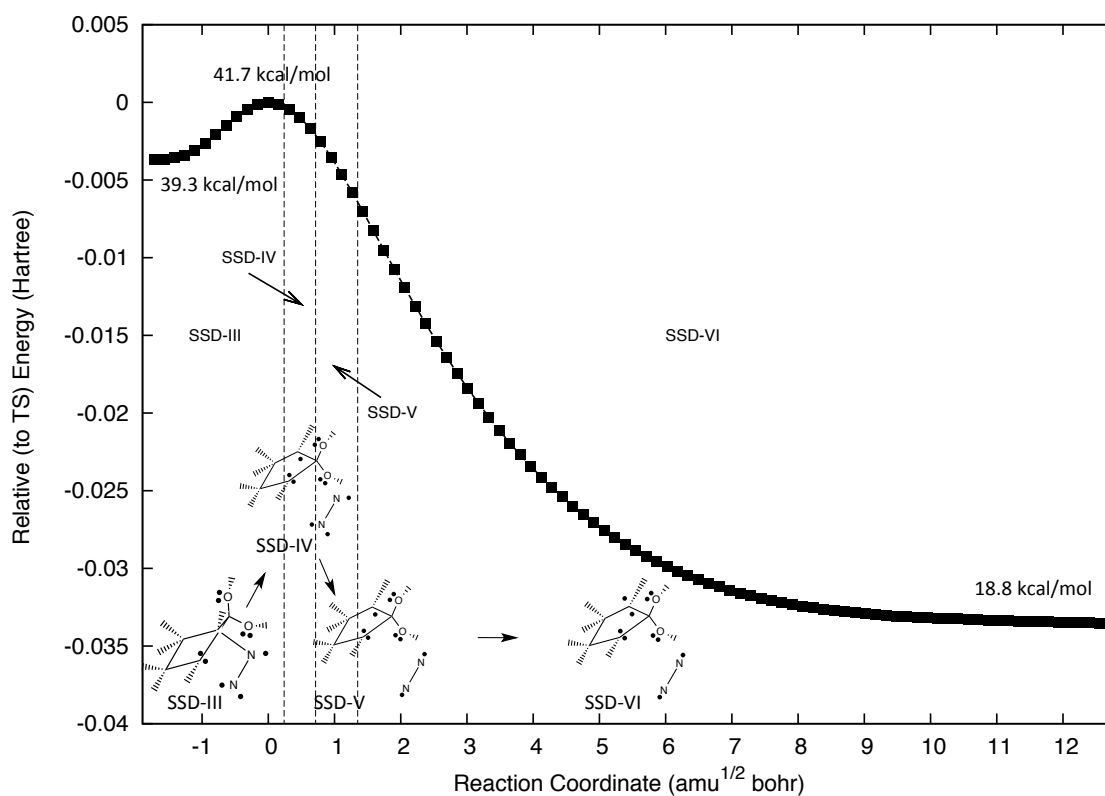
However, the thermal migration process of DBOH entails one more step (SSDs), making this thermal rearrangement more complex and energetically less favourable, see Table 1. Indeed, the C-N bond cleavages occur in different stages of process. Upon the first C2-N1 bond cleavage, the system continues with some basin rearrangements until reaching the second C-N bond breaking. Therefore, the presence of the OH substituents certainly does not favour the migration rearrangement. Furthermore, the OH migration takes place along two SSDs, while the hydride migration is completed within a single SSD. In both cases, the migration process is not completed until the formation of the double bond between C2 and C3 is reached.

d) Denitrogenation of DBOH via *stepwise* reaction pathway

The energy profile for this pathway and its six SSDs are depicted in Figures 12a and 12b. Figure 12a corresponds to the energy profile from DBOH (left side) towards DZ-DBOH species (right side) via TSS1-DBOH. Figure 12b corresponds to the energy profile from DZ-DBOH (left side) towards DBOH-diyl (right side) via TSS2-DBOH. It is worth mentioning that two structures for DZ-DBOH have been predicted for each energy profile. They do not exactly match, because they exhibit different rotation angle around the C4-N2 bond. However, their ELF topologies are the same, and hence belong to the same SSD, see below. In addition, the populations for the different basins are very similar in either conformation, as can be qualitatively sensed in the Figures 13a (right side) and 13b (left side). From a quantitative viewpoint, the maximum discrepancy (of only 0.1 e) has been found for the V(N2) basin population. The SSDs found are sketched in the Figures 12 from the perspective of ELF analysis. The populations of some basins are shown in Figure 13, while snapshots of the ELF localization domains for some selected points along the pathway from DBOH to DBOH-diyl, representative of the different SSDs are presented in Figure 14.

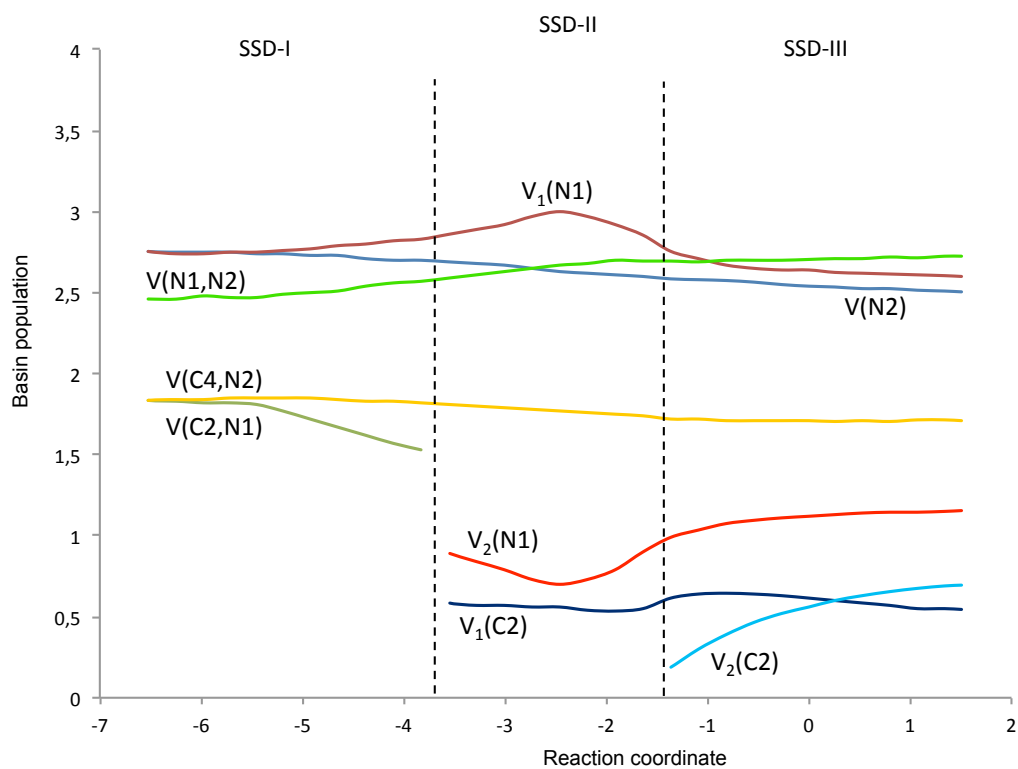


(a)

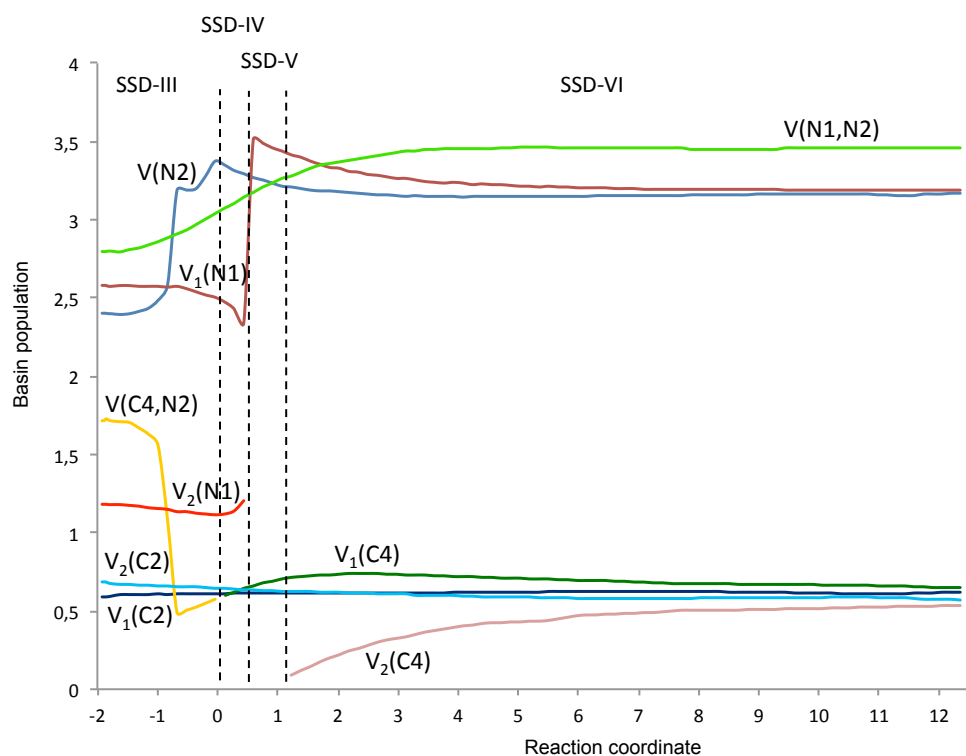


(b)

Figure 12. (a) Energy profile for the denitrogenation of DBOH (left side) to give DZ-DBOH (right side), via TSS1-DBOH species, and (b) energy profile for the DZ-DBOH (left side) evolution to the DBOH-diyl species plus N_2 (right side), via TSS2-DBOH. Both energy profiles have been calculated by means of the IRC method. The SSDs topology obtained from the BET analysis are sketched.



(a)



(b)

Figure 13. (a) Population evolution of some basins along the IRC from DBOH to DZ-DBOH, and (b) population evolution of some basins along the IRC of the DBOH denitrogenation process *via* the *stepwise* reaction pathway, both as a function of the reaction coordinate ($\text{amu}^{1/2} \text{ bohr}$).

An analysis of the results points out that the first ELF topological change accounts for the C2-N1 bond cleavage. As consequence, the population of the disynaptic basin $V(N1,N2)$ only increases 0.12e. The split of the disynaptic basin $V(C2,N1)$ into two monosynaptic basins $V_1(C2)$ and $V_2(N1)$ (cusp-type catastrophe) is observed when the SSD-II is reached (see Figure 13a). Upon the C2-N1 bond cleavage the system undergoes an excess of charge density on C2 which is reflected in the creation of a new monosynaptic basin $V_2(C2)$ (fold-type catastrophe) when the SSD-III is reached. Note that TSS1-DBOH, DZ-DBOH and TSS2-DBOH belong to the same SSD. Then, in the course of the SSD-III a pronounced increase of the population of the monosynaptic basin $V(N2)$ (Figure 13b) is observed and, in contrast, a decrease in the population of the disynaptic basin $V(C4,N2)$ is also sensed. The disynaptic basin $V(N1,N2)$ increases its population up to 2.71e at TSS1-DBOH, 2.76e (avg.) at DZ-DBOH, and 3.00e at TSS2-DBOH). Subsequently, the annihilation of the disynaptic basin $V(C4,N2)$ is sensed when the SSD-IV is reached. Interestingly, the second C-N bond cleavage takes place immediately after the system overcomes the TSS2-DBOH. The SSD-IV is very short and principally reflects a pronounced change in the population of the monosynaptic basin $V_1(N1)$. As result, the annihilation of the monosynaptic basin $V_2(N1)$ occurs when the SSD-V is reached. Finally, the last ELF topological change arises as consequence of an excess of charge density on C4 which is reflected in the creation of the monosynaptic basin $V_2(C4)$ (fold-type catastrophe) when SSD-VI is reached.

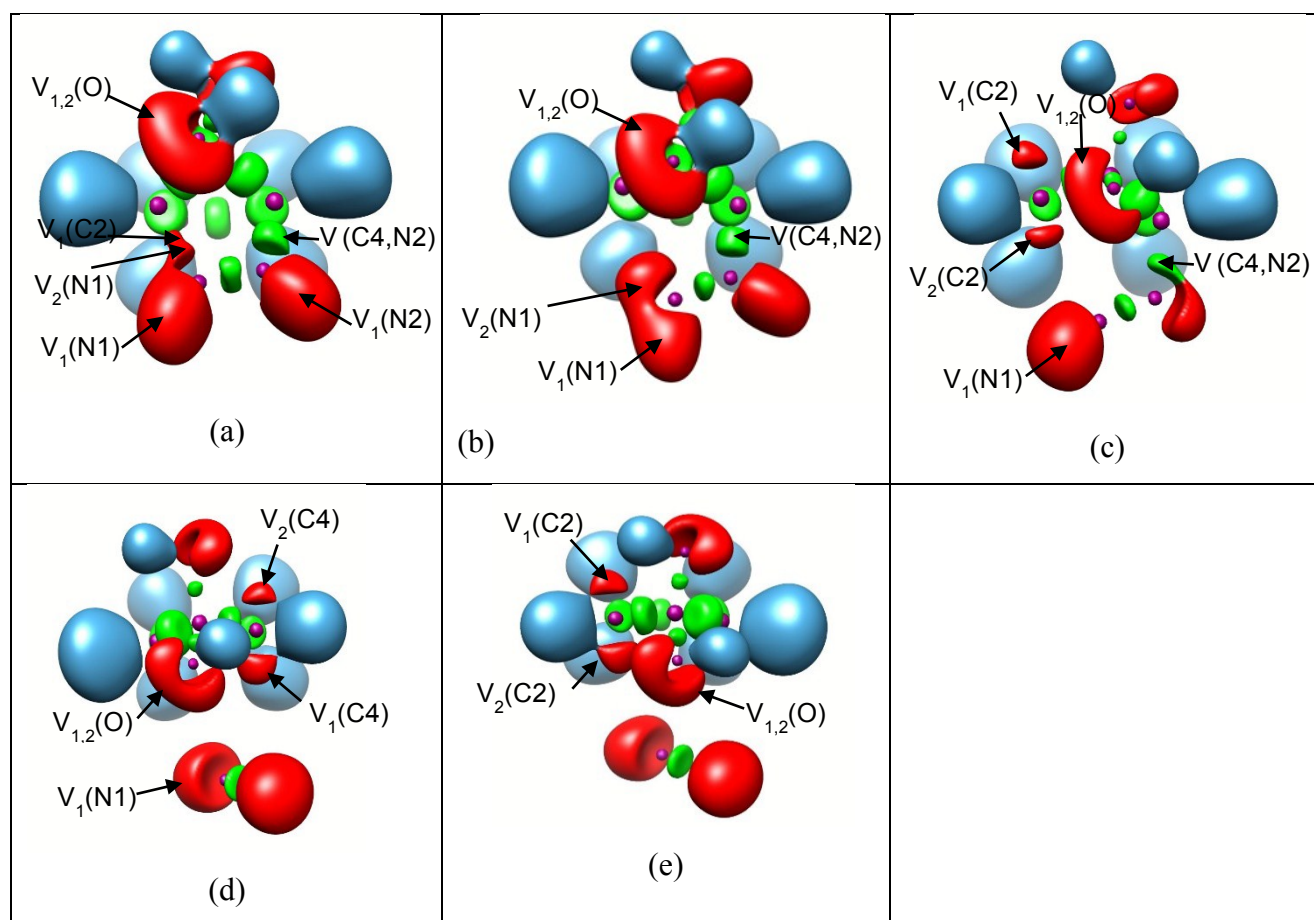


Figure 14. Snapshots of the ELF localization domains ($\eta = 0.8$ isosurface except where indicated) for selected points along the IRC of the DBOH denitrogenation process *via* the *stepwise* reaction pathway (see DBOH belonging to SSD-I in Figure 11a). (a) Point belonging to SSD-II; (b) TSS1 belonging to SSD-III (alpha electrons); (c) TSS1 belonging to SSD-III ($\eta = 0.857$ isosurface beta electrons). (d) DBOH-diyl species plus N_2 , belonging to SSD-VI ($\eta = 0.84$ isosurface, alpha electrons); (e) DBOH-diyl species plus N_2 , belonging to SSD-VI ($\eta = 0.84$ isosurface, beta electrons).

The DBH *concerted* pathway and the DBOH *stepwise* pathway can be compared since both denitrogenation processes result in DBH-diyl and the DBOH-diyl species. As described, the presence of two hydroxyl groups on C3 dramatically alters the denitrogenation process. In the DBH case the C-N bond cleavages occur simultaneously, confirmed with the present ELF topological study. Four SSDs have been characterized accounting for the chemical events that take place in the way from DBH to DBH-diyl. However, in the DBOH case one of the C-N bonds break first, initiating a cascade of chemical events that take place in the way from DBOH to DBOH-diyl, including a transition structure that makes possible the formation of the intermediate DZ-DBOH, the passage through a second transition structure accounting for the second C-N bond breaking, and the final electronic rearrangements to reach the final DBOH-diyl species.

Interestingly, the population of the disynaptic basin $V(N1,N2)$ can provide a good

correlation with experiments. Indeed, when the simultaneous C-N bond cleavages take place in DBH the population of the disynaptic basin $V(N1,N2)$ is predicted to be 2.63e, whereas for the DBOH these are predicted to be 2.58e and 3.06e in the first and the second C-N bond cleavage, respectively. The greater population of the disynaptic basin $V(N1,N2)$ before the first C-N breaking found for the DBH correlates with the experimental observation of a greater wavenumber observed for the N=N stretching in the DBH (1950 cm^{-1}) compared to DBOH (1750 cm^{-1}). This also holds true in this basin population of the respective transition states and intermediates (at TSc-DBH = 2,97e; at TSS1-DBOH = 2,70e; at DZ-DBOH = 2,76e; at TSS2-DBOH = 3,00e)

Finally, a last question remains to be answered: can the topological analysis shed some additional light in what refers to why the presence of the OH substituents push the denitrogenation process through a stepwise mechanism instead of through a concerted process? We have not found neither a *concerted* process for the denitrogenation of the DBOH, nor a *stepwise* mechanism for the denitrogenation of DBH, and hence we cannot make a direct comparative analysis. However, the answer to that question should be intimately related to the answer of this alternative one: why the C-N bonds do break simultaneously in the DBH denitrogenation processes and consecutively in the DBOH case? The analysis of the population values of the disynaptic $V(C2,N1)$ and $V(C4,N2)$ basins along the reaction coordinate provides the desired clues: in both DBH denitrogenation processes, the population of the disynaptic basin $V(C2,N1)$ is maintained always identical to the population of the $V(C4,N2)$ basin, likewise the molecular symmetry that is maintained until these disynaptic basins disappear accounting for the C-N ruptures. Therefore, the N_2 departure takes place in a concerted manner without symmetry loose. It should be noted that in the *migration* mechanism the H motion takes place *after* the N_2 departure, as has been shown, and hence the inherent symmetry loose associated with this H displacement does not affect the C-N ruptures. However, in the DBOH denitrogenation processes, the population values of these disynaptic basins are slightly different to each other from the very beginning. And, as it is apparent from figures 10 and 13a, the basin with the initial lowest population of these two basins is the one that disappears first. The population difference must be due to the particular orientation of the monosynaptic $V(O)$ basins belonging to the OH substituents on C3 (see figure 11a), that are not symmetrically placed and influence in different manner the two molecule moieties, pushing and pulling the electron flow and making the two C-N bonds different. Hence, the reason for the asynchronous rupture of the two C-N bonds in the DBOH denitrogenation processes would lie on the asymmetry in the population of the $V(C,N)$ basins, which in turn is caused by the particular orientation of the $V(O)$ monosynaptic basins of the OH substituents on C3. In this way, one of the C-N bonds breaks first and therefore a different topological description of the denitrogenation processes of DBOH is obtained which involve more

SSDs compared to DBH. We have included in the supporting material the cartesian coordinates of the optimized DBH and DBOH.

4. Conclusions

All stages of the denitrogenation processes of 2,3 diazabicyclo[2.2.1]hept-2-ene derivatives have been studied by means of BET, based on topological analysis of ELF and CT. This procedure yields substantial information about chemical bonding along the reaction pathway, and allows us to investigate in detail the corresponding reaction pathways and to understand the flow of electrons that attends the process. From the experimental side, this chemical reaction has been analysed by a visible 5-fs pulse laser, allowing the characterization of the time-dependent frequency shifts of relevant molecular vibrational modes, that can be related to the progress of the $V(N1,N2)$ basin population along the reaction pathway. Our results are capable to explain why the DBH denitrogenation takes place via a simultaneous C-N bond breaking mechanism, and rationalize the observations made for the DBH concerted denitrogenation pathway compared to the stepwise DBOH denitrogenation process.

A concerted denitrogenation process was found in the thermolysis of the DBH; however, a stepwise nitrogen dissociation process was obtained for the denitrogenation process of the DBOH. Present theoretical results agree well with the experimental predictions, and the main conclusions of the present work can be summarized as follows: i) we have for the first time (to our knowledge) characterized the TSs for the denitrogenation of DBH derivatives through migration-type pathways, ii) we have noticed that the use of the extended basis set is necessary for the characterization of some stationary points along the reaction processes. iii) The description that emerges from BET analysis of the DBH migration pathway reveals that the first chemical event is the simultaneous two C-N bonds breaking process. After that, the next chemical event corresponds to the hydride migration process that becomes apparent when the reaction has advanced halfway. The double C3-C4 bond development is the last chemical event along the whole process. iv) For the DBH concerted pathway the same behaviour can be observed: the process begins with the simultaneous C-N bond breaking process, and the rest of the events take place well afterwards and mainly affect the monosynaptic basins, v) the presence of the OH substituents greatly changes the intimate electronic mechanism for the migration pathway and the C-N bond breaking processes takes place in two different stages of the process. The series of chemical events begin with the breaking of one C-N bond, continues with some basin rearrangements before the second C-N bond breaks, thereafter the OH leaves and its migration is not completed until the double bond formation has taken place, vi) on the other hand, for the DBOH *stepwise* denitrogenation process, it can be sensed

that TSS1-DBOH is very late with respect to the first C-N bond breaking process, and from the ELF electronic point of view, TSS1-DBOH shares the same topological domain with DZ-DBOH and TSS2-DBOH. Interestingly, the breaking process of the C4-N2 occurs immediately after the system overcomes the TSS2-DBOH. Also in this case, as it happened with the migration pathway, the presence of the two hydroxyl groups on C3 completely changes the reaction mechanism for the denitrogenation processes leading to the diradical intermediate: in the DBH case the two C-N bonds break simultaneously, and four SSDs have been characterized accounting for the chemical events that take place in the way from DBH to DBH-diyl. However, in the DBOH case one of the C-N bonds breaks first, initiating a cascade of chemical events that take place in the way from DBOH to DBOH-diyl, including a transition structure that makes possible the formation of the intermediate DZ-DBOH, its configuration change, the passage through a second transition structure accounting for the second C-N bond breaking, and the final electronic rearrangements to reach the final DBOH-diyl species, vii) the evolution of the population of the V(N1,N2) disynaptic basin can be related with the experimental data relative to the N₂ release, and our results nicely correlate with the experimental findings explaining why the N₂ release is easier for DBH via a *concerted* mechanism compared to the *stepwise* mechanism found in DBOH viii) Our results suggest that the reason for the different denitrogenation mechanisms (*concerted versus stepwise*) taking place in these systems would lie on the asymmetry in the initial population of the V(C,N) basins, which in turn is caused by the particular orientation of the V(O) monosynaptic basins of the OH substituents on C3.

The calculations have thus provided a deep insight into the nature of the denitrogenation processes. This is a nice guide study to elucidate the mechanism of chemical reactions, and it is a critical step in the analysis of reaction pathways and rates.

Supporting information available. Tables 1S and 2S with relative energy values for the stationary points found at four theoretical levels. Figures 1S to 4S with the ELF localization domains snapshots for points representing all SSDs found. DBH and DBOH cartesian coordinates. ELF mathematical model.

5. Acknowledgments

The authors are grateful to Generalitat Valenciana for *PrometeoII/2014/022* and *ACOMP/2015/102* projects, Ministerio de Economía y Competitividad (Spain) for project CTQ-2012-36253-C03-02, and Universitat Jaume I for project P1·1B2013-40. The authors are also grateful to the Servei d'Informàtica, Universitat Jaume I for generous allocation of computer time. P.G-N acknowledges support from the Alexander von Humboldt Foundation.

6. References

1. H. N. Chapman, P. Fromme, A. Barty, T. A. White, R. A. Kirian, A. Aquila, M. S. Hunter, J. Schulz, D. P. DePonte, U. Weierstall, R. B. Doak, F. R. N. C. Maia, A. V. Martin, I. Schlichting, L. Lomb, N. Coppola, R. L. Shoeman, S. W. Epp, R. Hartmann, D. Rolles, A. Rudenko, L. Foucar, N. Kimmel, G. Weidenspointner, P. Holl, M. Liang, M. Barthelmess, C. Caleman, S. Boutet, M. J. Bogan, J. Krzywinski, C. Bostedt, S. Bajt, L. Gumprecht, B. Rudek, B. Erk, C. Schmidt, A. Hömke, C. Reich, D. Pietschner, L. Strüder, G. Hauser, H. Gorke, J. Ullrich, S. Herrmann, G. Schaller, F. Schopper, H. Soltau, K.-U. Kühnel, M. Messerschmidt, J. D. Bozek, S. P. Hau-Riege, M. Frank, C. Y. Hampton, R. G. Sierra, D. Starodub, G. J. Williams, J. Hajdu, N. Timneanu, M. M. Seibert, J. Andreasson, A. Rocker, O. Jönsson, M. Svenda, S. Stern, K. Nass, R. Andritschke, C.-D. Schröter, F. Krasniqi, M. Bott, K. E. Schmidt, X. Wang, I. Grotjohann, J. M. Holton, T. R. M. Barends, R. Neutze, S. Marchesini, R. Fromme, S. Schorb, D. Rupp, M. Adolph, T. Gorkhover, I. Andersson, H. Hirsemann, G. Potdevin, H. Graafsma, B. Nilsson and J. C. H. Spence, *Nature*, 2010, **470**, 73-77.
2. F. Krausz and M. Ivanov, *Rev. Mod. Phys.*, 2009, **81**, 163-234.
3. M. Abe, I. Iwakura, A. Yabushita, S. Yagi, J. Liu, K. Okamura and T. Kobayashi, *Chem. Phys. Lett.*, 2012, **527**, 79-83.
4. I. Iwakura, *Phys. Chem. Chem. Phys.*, 2011, **13**, 5546-5555.
5. I. Iwakura, A. Yabushita and T. Kobayashi, *Chem. Lett.*, 2010, **39**, 374-375.
6. P. S. Engel, *Chem. Rev.*, 1980, **80**, 99-150.
7. W. R. Roth and M. Martin, *Liebigs. Ann. Chem.*, 1967, **702**, 1.
8. W. R. Roth and M. Martin, *Tetrahedron Lett.*, 1967, 4695-4698.
9. E. L. Allred and R. L. Smith, *J. Am. Chem. Soc.*, 1969, **91**, 6766-6775.
10. W. Adam, T. Oppenlander and G. Zang, *J. Org. Chem.*, 1985, **50**, 3303-3312.
11. B. A. Lyons, J. Pfeifer, T. H. Peterson and B. K. Carpenter, *J. Am. Chem. Soc.*, 1993, **115**, 2427-2437.
12. M. B. Reyes and B. K. Carpenter, *J. Am. Chem. Soc.*, 1998, **120**, 1641-1642.
13. N. Yamamoto, M. Olivucci, P. Celani, F. Bernardi and M. A. Robb, *J. Am. Chem. Soc.*, 1998, **120**, 2391-2407.
14. W. Adam, H. Garcia, V. Marti and J. N. Moorthy, *J. Am. Chem. Soc.*, 1999, **121**, 9475-9476.
15. M. B. Reyes and B. K. Carpenter, *J. Am. Chem. Soc.*, 2000, **122**, 10163-10176.
16. A. Sinicropi, C. S. Page, W. Adam and M. Olivucci, *J. Am. Chem. Soc.*, 2003, **125**, 10947-10959.
17. W. Adam, M. Diederich and A. V. Trofimov, *J. Phys. Org. Chem.*, 2004, **17**, 643-655.
18. M. Abe, C. Ishihara, S. Kawanami and A. Masuyama, *J. Am. Chem. Soc.*, 2005, **127**, 10-11.
19. S. Yagi, Y. Hiraga, R. Takagi and M. Abe, *J. Phys. Org. Chem.*, 2011, **24**, 894-901.
20. K. S. Khuong and K. N. Houk, *J. Am. Chem. Soc.*, 2003, **125**, 14867-14883.
21. M. Hamaguchi, M. Nakaishi, T. Nagai, T. Nakamura and M. Abe, *J. Am. Chem. Soc.*, 2007, **129**, 12981-12988.
22. C. Ishihara and M. Abe, *Aust. J. Chem.*, 2010, **63**, 1615-1618.
23. P. L. A. Popelier and E. A. G. Bremond, *Int. J. Quantum Chem.*, 2009, **109**, 2542-2553.
24. R. F. W. Bader, *Atoms in molecules : a quantum theory*, Clarendon Press Oxford New York, 1990.
25. R. F. W. Bader, T. T. Nguyendang and Y. Tal, *Rep. Prog. Phys.*, 1981, **44**, 893-948.
26. X. Krokidis, S. Noury and B. Silvi, *J. Phys. Chem. A*, 1997, **101**, 7277-7282.
27. A. D. Becke and K. E. Edgecombe, *J. Chem. Phys.*, 1990, **92**, 5397-5403.
28. B. Silvi and A. Savin, *Nature*, 1994, **371**, 683-686.

29. R. Thom, *Structural stability and morphogenesis; an outline of a general theory of models*, W. A. Benjamin, Reading, Mass., [1st English edn., 1975.
30. V. Polo, P. Gonzalez-Navarrete, B. Silvi and J. Andres, *Theor. Chem. Acc.*, 2008, **120**, 341-349.
31. J. Andres, S. Berski, L. R. Domingo and P. Gonzalez-Navarrete, *J. Comput. Chem.*, 2012, **33**, 748-756.
32. P. Gonzalez-Navarrete, L. R. Domingo, J. Andres, S. Berski and B. Silvi, *J. Comput. Chem.*, 2012, **33**, 2400-2411.
33. P. Gonzalez-Navarrete, F. R. Sensato, J. Andres and E. Longo, *J. Phys. Chem. A*, 2014, **118**, 6092-6103.
34. J. Andres, S. Berski, L. R. Domingo, V. Polo and B. Silvi, *Curr. Org. Chem.*, 2011, **15**, 3566-3575.
35. S. Berski, F. R. Sensato, V. Polo, J. Andres and V. S. Safont, *J. Phys. Chem. A*, 2011, **115**, 514-522.
36. V. Polo, J. Andres, S. Berski, L. R. Domingo and B. Silvi, *J. Phys. Chem. A*, 2008, **112**, 7128-7136.
37. V. Polo and J. Andres, *J. Comput. Chem.*, 2005, **26**, 1427-1437.
38. V. Polo, J. Andres, R. Castillo, S. Berski and B. Silvi, *Chem. Eur. J.*, 2004, **10**, 5165-5172.
39. V. Polo, J. Andres and B. Silvi, *J. Comput. Chem.*, 2007, **28**, 857-864.
40. V. Polo, L. R. Domingo and J. Andres, *J. Phys. Chem. A*, 2005, **109**, 10438-10444.
41. V. Polo, L. R. Domingo and J. Andres, *J. Org. Chem.*, 2006, **71**, 754-762.
42. J. C. Santos, J. Andres, A. Aizman, P. Fuentealba and V. Polo, *J. Phys. Chem. A*, 2005, **109**, 3687-3693.
43. P. González-Navarrete, J. Andrés and S. Berski, *J. Phys. Chem. Lett.*, 2012, **3**, 2500-2505.
44. M. J. Frisch, H. B. Schlegel, G. E. Scuseria, J. R. C. M. A. Robb, G. Scalmani, V. Barone, B. Mennucci, H. N. G. A. Petersson, M. Caricato, X. Li, H. P. Hratchian, J. B. A. F. Izmaylov, G. Zheng, J. L. Sonnenberg, M. Hada, K. T. M. Ehara, R. Fukuda, J. Hasegawa, M. Ishida, T. Nakajima, O. K. Y. Honda, H. Nakai, T. Vreven, J. A. Montgomery, Jr., F. O. J. E. Peralta, M. Bearpark, J. J. Heyd, E. Brothers, V. N. S. K. N. Kudin, T. Keith, R. Kobayashi, J. Normand, A. R. K. Raghavachari, J. C. Burant, S. S. Iyengar, J. Tomasi, N. R. M. Cossi, J. M. Millam, M. Klene, J. E. Knox, J. B. Cross, C. A. V. Bakken, J. Jaramillo, R. Gomperts, R. E. Stratmann, A. J. A. O. Yazyev, R. Cammi, C. Pomelli, J. W. Ochterski, K. M. R. L. Martin, V. G. Zakrzewski, G. A. Voth, J. J. D. P. Salvador, S. Dapprich, A. D. Daniels, J. B. F. O. Farkas, J. V. Ortiz, J. Cioslowski, and G. and D. J. Fox, Gaussian 09, Inc., Wallingford CT, 2010.
45. A. D. Becke, *Phys Rev A*, 1988, **38**, 3098-3100.
46. A. D. Becke, *J. Chem. Phys.*, 1993, **98**, 5648.
47. C. T. Lee, W. T. Yang and R. G. Parr, *Physical Review B*, 1988, **37**, 785-789.
48. Y. Zhao, N. E. Schultz and D. G. Truhlar, *J. Chem. Theory. Comput.*, 2006, **2**, 364-382.
49. K. Fukui, *J. Phys. Chem.*, 1970, **74**, 4161-4163.
50. K. Fukui, *Acc. Chem. Res.*, 1981, **14**, 363-368.
51. S. Noury, X. Krokidis, F. Fuster and B. Silvi, *Comput. Chem.*, 1999, **23**, 597-604.
52. E. F. Pettersen, T. D. Goddard, C. C. Huang, G. S. Couch, D. M. Greenblatt, E. C. Meng and T. E. Ferrin, *J. Comput. Chem.*, 2004, **25**, 1605-1612.
53. R. Bauernschmitt and R. Ahlrichs, *J. Chem. Phys.*, 1996, **104**, 9047-9052.
54. R. Caballol, O. Castell, F. Illas, P. R. Moreira and J. P. Malrieu, *J. Phys. Chem. A*, 1997, **101**, 7860-7866.
55. L. Noodleman, *J. Chem. Phys.*, 1981, **74**, 5737-5743.
56. J. Andres, P. Gonzalez-Navarrete and V. Sixte Safont, *Int. J. Quantum. Chem.*, 2014, **114**, 1239-1252.
57. J. Andrés, L. Gracia, P. González-Navarrete and V. S. Safont, *Comput. Theor. Chem.*, 2015, **1053**, 17-30.

58. B. Silvi, *Journal of Molecular Structure*, 2002, **614**, 3-10.
59. S. Berski, J. Andres, B. Silvi and L. R. Domingo, *J. Phys. Chem. A*, 2006, **110**, 13939-13947.
60. J. Melin and P. Fuentealba, *Int. J. Quatum. Chem.*, 2003, **92**, 381-390.
61. I. Viciano, P. González-Navarrete, J. Andrés and S. Martí, *J. Chem. Theory. Comput.*, 2015, **11**, 1470-1480.